ChemPubSoc Europe

DOI: 10.1002/batt.201900069

BATTERIES & SUPERCAPS
Communications

Enhancing the Rate Capability of Niobium Oxide Electrode through Rare-Earth Doping Engineering

Dandan Yin[+],[a] Hongyang Zhao[+],[a, b] Na Li,[c] Rui Si,[d] Xiaolei Sun,[a] Xinghua Li,[e] and Yaping Du*[a]

Dedicated to 100th Anniversary of Nankai University

Niobium oxide is considered one of the most promising electrode materials for ultrafast electrochemical energy storage devices with high energy density. In this work, we first found that trace amounts (<1%) of Yb^{3+} doping remarkably enhanced the rate capability of T–Nb_2O_5, which was further proved to be because of the formation of a thin layer of amorphous $YbNbO_x$. The capacity of $YbNbO_x$-coated Nb_2O_5 reached 124 mAh g^{-1} at 20 C, which is the highest value reported among pristine Nb_2O_5 electrodes. Besides, we found that doping with other rare-earth elements such as Nd^{3+}, Sm^{3+}, and Gd^{3+} can also improve the rate capability of T–Nb_2O_5. It can be concluded that rare-earth doping can be an effective and robust method to enhance the intrinsic rate performance of electrode materials without complicated modifications.

Niobium (V) oxide is an important family of electrode material with excellent lithium ion storage properties. Among various polymorphs of Nb_2O_5, i.e., H–Nb_2O_5, M–Nb_2O_5, T–Nb_2O_5 and TT–Nb_2O_5, T–Nb_2O_5 has the best rate capability even without nanosizing compared with other polymorphs.[1] The excellent rate performance is attributed to lithium ion transport through 1D channel along the b-axis of T–Nb_2O_5 crystal with extremely small diffusion hinderance.[2] Therefore, T–Nb_2O_5 has attracted most of the attention in niobium oxide family for high rate lithium storage. Many approaches have been applied to further improve its performance. The most common way is to composite T–Nb_2O_5 with conductive material to enhance its electric contact.[3] It was reported that freestanding Nb_2O_5 nanowire array grown on conductive substrate and T–Nb_2O_5 nanoparticles anchored on graphene paper showed enhanced rate capability.[4] One of the representative examples was reported by Duan et al. that porous graphene hydrogel/T–Nb_2O_5 nanoparticles could achieve extremely high area capacity of 4 mAh cm^{-2} and volumetric capacity of 280 mAh cm^{-3}.[5] The high energy density of the composite is attributed to the increased conductivity as well as special porous structure. Another way to better rate performance is morphological control. Nb_2O_5 nanosheets, nanofibers, and mesoporous Nb_2O_5 showed much higher performance compared with the bulk counterpart.[6] However, besides structural design and conductive coating, it is very challenging to enhance the intrinsic electrochemical performance of Nb_2O_5 to approach the theoretical limits for high rate.

Generally, T–Nb_2O_5 is a layered structure with alternating atom-dense (4 h) layers and atom-sparse (4 g) layers. The lithium ion transports in 4 g layer with low-hinderance which results in the ultrafast lithium ion transport.[2] The charges store in T–Nb_2O_5 with a Li^+ intercalation pseudocapacitance mechanism and the rate capability of T–Nb_2O_5 is exceptionally good.[7] The lithium migration hindrance is closely related to the local coordination environment. Aiming at increasing the intrinsic performance of electrode material, surface doping by coating metal oxides offers an important way to further enhance the rate capability by reducing inter-particle resistance as well as tuning the structure of original electrode material. It is widely reported that surface coating layer would generally reduce polarization at high current density.[8]

Rare-earth elements are candidates for both matrix material and doping species for high-performance solid-state electrolyte.[9] In this contribution, we studied the electrode diffusion behavior and the chemical environment of rare-earth element in electrode materials. Importantly, we found that trace amount (<1%) of Yb^{3+} addition could significantly enhance the rate capability of T–Nb_2O_5 by forming an amorphous $YbNbO_x$ layer.

The electrode material was synthesized by a facile sol-gel method with assistance of block polymer surfactant.[10] Rare-earth element incorporation was achieved by adding a certain

[a] D. Yin,[+] H. Zhao,[+] X. Sun, Prof. Y. Du
School of Materials Science and Engineering &
National Institute for Advanced Materials
Tianjin Key Lab for Rare Earth Materials and Application
Centre for Rare Earth and Inorganic Functional Materials
Nankai University, Tianjin 300350, P.R. China
E-mail: ypdu@nankai.edu.cn
[b] H. Zhao[+]
School of science, Xi'an Jiaotong University
Xi'an, Shaanxi 710054, P.R. China
[c] N. Li
Frontier Institute of Science and Technology
Xi'an Jiaotong University
Xi'an, Shaanxi 710054, P.R. China
[d] Prof. R. Si
Shanghai Synchrotron Radiation Facility
Shanghai Institute of Applied Physics
Chinese Academy of Sciences
Shanghai 201204, P.R. China
[e] Prof. X. Li
School of Physics, Northwest University
Xi'an, Shaanxi 710127, P.R. China
[+] These authors contributed equally to this work.

Supporting information for this article is available on the WWW under https://doi.org/10.1002/batt.201900069

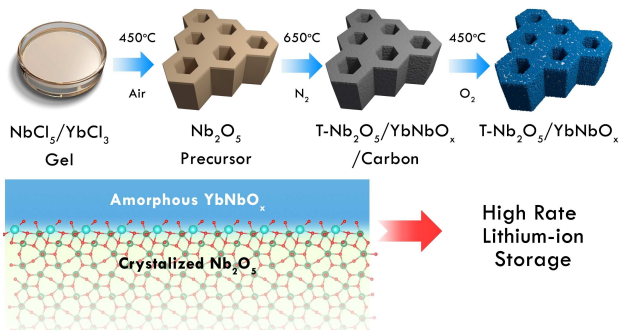

Figure 1. Schematic illustration of the preparation of T–Nb_2O_5/$YbNbO_x$ mesoporous electrode material.

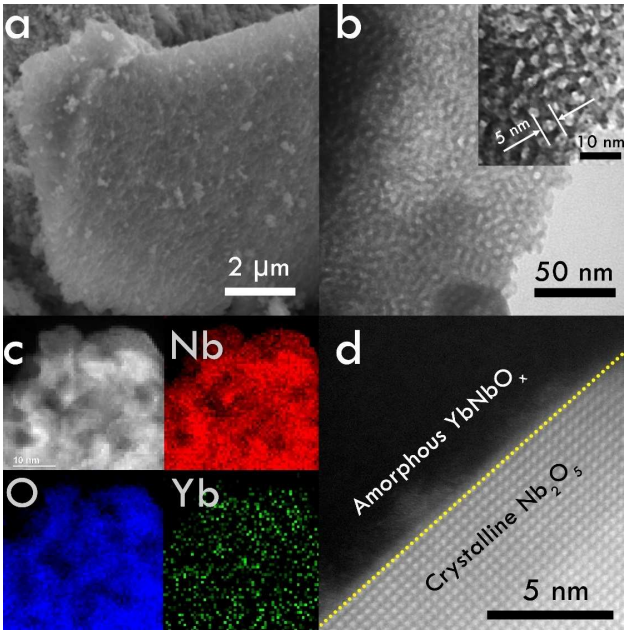

Figure 2. (a) SEM and (b) TEM image of mesoporous T–Nb_2O_5/$YbNbO_x$, the mesopore diameter was around 5 nm. (c) EELS mapping of T–Nb_2O_5/$YbNbO_x$. (d) Aberration corrected TEM image of T–Nb_2O_5/$YbNbO_x$.

amount of ethanol solution of rare-earth salt in to the initial sol. The material was obtained by firstly calcination in nitrogen at 650 °C to generate T–Nb_2O_5 phase without destruction of the porous structure and followed by calcination at 450 °C in oxygen to remove residual carbon (Figure 1). The scanning electron microscopy (SEM) image showed that the material was micrometer sized particles (Figure 2a). The electrode material has relatively large tap density of 1.06 g cm^{-3}, which was beneficial to its volumetric energy density. Closer examination was conducted on a transmission electron microscope (TEM). The TEM image showed that the material has regular mesopores with diameter of ~5 nm (Figure 2b, inset). These mesopores facilitate electrolyte penetrating the material during charge/discharge process. Electron energy loss spectroscopy (EELS) mapping showed that the ytterbium was homogenously distributed in the material, indicating Yb was coated on T–Nb_2O_5 (Figure 2c). We also performed aberration corrected TEM to check the rare-earth element in T–Nb_2O_5. Unfortunately, the Yb atoms cannot be distinguished in the microcopy, which may be attributed to the amorphous nature of $YbNbO_x$. It can also be found in Figure 2d that the crystal lattice of T–Nb_2O_5 showed perfect orthorhombic structure without lattice distortion in the bulk, and there is a thin coating layer of 1–2 nm on T–Nb_2O_5 surface, which can be considered as amorphous $YbNbO_x$. This justified that $YbNbO_x$ were homogeneously coated on the T–Nb_2O_5 surface.

The X-ray photoelectron spectroscopy (XPS) results of Nb 3d signals in T–Nb_2O_5 and T–Nb_2O_5/$YbNbO_x$ were presented in Figure 3a, it was concluded the Nb signal did not change with the addition of Yb. The Yb 4d signal in the T–Nb_2O_5/$YbNbO_x$ indicated the existence of ytterbium (Figure 3b). X-ray diffraction (XRD) measurement was conducted to study the phase and crystallinity of the samples. We tested three samples with different doping amount. The peaks of all samples can be attributed to the T–Nb_2O_5 (JCPDS-30873) with orthorhombic phase. Addition of Yb could barely affect the structure. Only when the Yb^{3+} amount increased to 10%, the XRD pattern showed a slight bias. Interestingly, it is worth to note that the Yb incorporation induced crystallinity decrease of T–Nb_2O_5 matrix. The intensity became slightly weaker with 1% of Yb^{3+} addition. When increased the doping amount to 10%, the material became nearly amorphous while there was no peak of Yb_2O_3 or other ytterbium-related oxides, which indicates the ytterbium oxide was amorphous. The decrease in XRD intensity implies more amorphous oxide would form during calcination with increasing Yb concentration (Figure 3c). Raman spectra of both T–Nb_2O_5/$YbNbO_x$ and pure T–Nb_2O_5 showed typical T–Nb_2O_5 bands generated by overlapping peaks. The Raman intensity of the T–Nb_2O_5/$YbNbO_x$ was similar to pure T–Nb_2O_5, indicating that the $YbNbO_x$ formation would not substantially change the crystal structure of the matrix (Figure 3d).

We tested the electrochemical properties of the pure T–Nb_2O_5 and T–Nb_2O_5/$YbNbO_x$ as electrode materials in lithium-ion batteries (LIBs). The performance of the pure Nb_2O_5 and T–Nb_2O_5/$YbNbO_x$ showed significant difference. Figure 4a showed the cyclic voltammetry (CV) of T–Nb_2O_5/$YbNbO_x$. The CV curves in increasing scan rates of 0.2, 0.5, 1, 2, 5, mV s^{-1} displayed typical symmetric peaks around 1.6-1.8 V when lithium ions inserting into T–Nb_2O_5. Increasing scan rate leads to small peak polarization compared with pure Nb_2O_5, indicating the excellent electrode kinetics (Figure S5). Charge/discharge curves of both pure T–Nb_2O_5 and T–Nb_2O_5/$YbNbO_x$ electrodes did not show much difference, which is further evidenced by the almost identical differentiated charge/discharge curves. The only difference in charge/discharge curves was that the capacity of T–Nb_2O_5/$YbNbO_x$ was larger than pure T–Nb_2O_5. However, the difference was small at low current density of 0.5 C (1 C = 201 mA g^{-1}) (Figure 4b). This indicated that surface coating could not improve its intrinsic capacity because the basic structure of T–Nb_2O_5 was not changed. Rate performance was measured from current density of 0.5 to 20 C. It can be seen from Figure 4c that at low current density, the pure T–Nb_2O_5 and T–Nb_2O_5/$YbNbO_x$ electrode showed small difference in capacity. With the increase of current density, T–Nb_2O_5/$YbNbO_x$ demonstrated much better

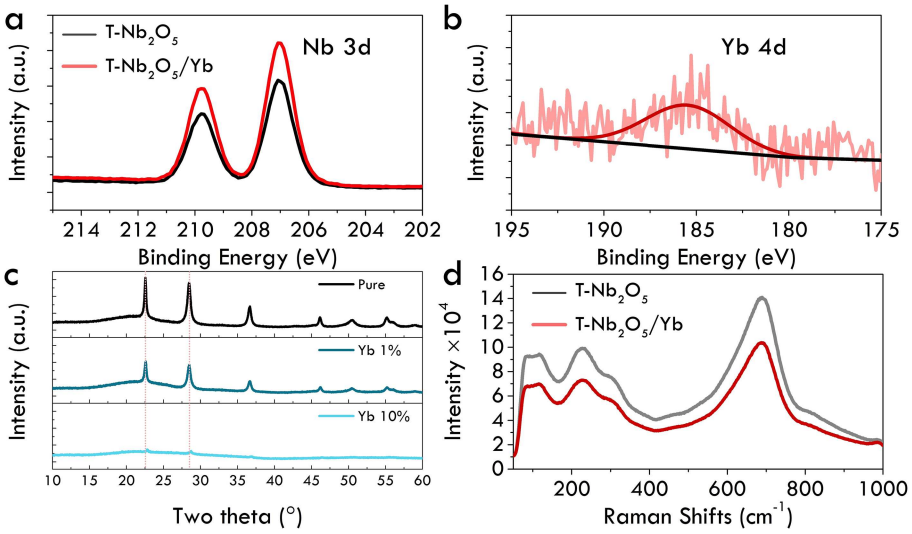

Figure 3. XPS results of (a) Nb 3d and (b) Yb 4d signals of T–Nb_2O_5 and T–Nb_2O_5/$YbNbO_x$. (c) XRD patterns of T–Nb_2O_5 and T–Nb_2O_5/$YbNbO_x$. (d) Raman spectra of T–Nb_2O_5 and T–Nb_2O_5/$YbNbO_x$.

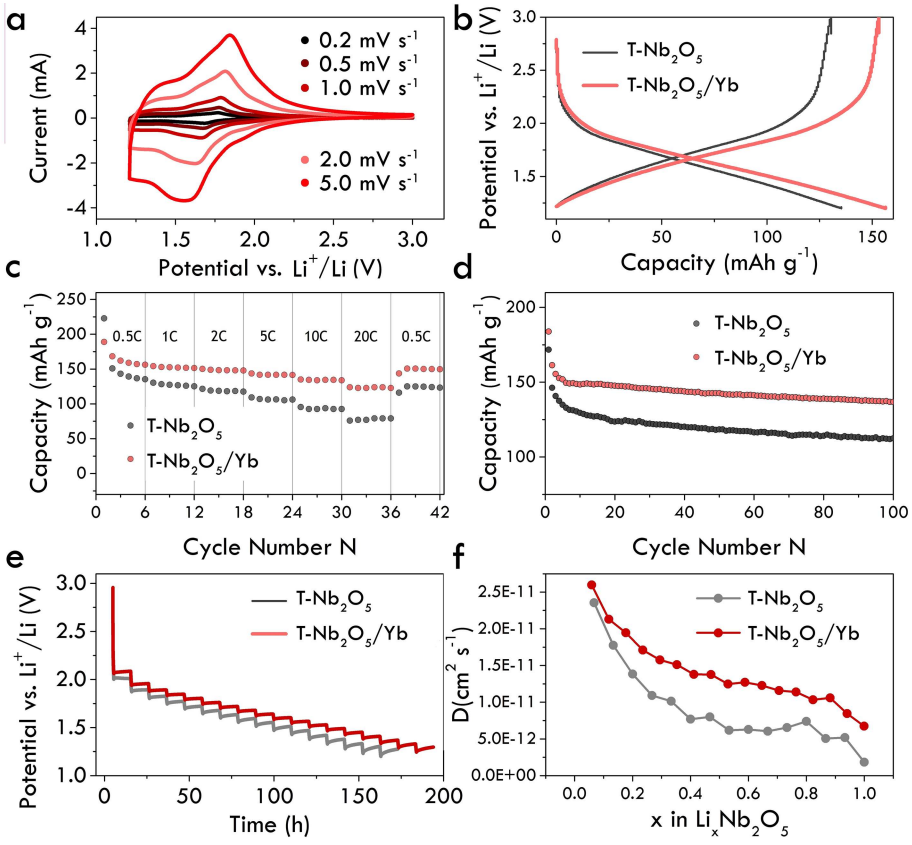

Figure 4. Electrochemical performance of T–Nb_2O_5 and T–Nb_2O_5/$YbNbO_x$. (a) Cyclic voltammetry of T–Nb_2O_5/$YbNbO_x$ at various scan rates. (b) Charge/discharge curves of T–Nb_2O_5 and Nb_2O_5-Yb at 0.5 C rate. (c) Rate performance of T–Nb_2O_5 and T–Nb_2O_5/$YbNbO_x$ at various current densities. (d) Cycle stability of T–Nb_2O_5 and T–Nb_2O_5/$YbNbO_x$ at a current density of 5 C. (e) Galvanostatic intermittent titration technique (GITT) measurement of T–Nb_2O_5 and T–Nb_2O_5/$YbNbO_x$. (f) Calculated diffusion coefficients at different discharge state of T–Nb_2O_5 and T–Nb_2O_5/$YbNbO_x$.

rate performance than pure T–Nb_2O_5. At high current density of 20 C, the capacity T–Nb_2O_5/$YbNbO_x$ still maintained at 124 mAh g^{-1}, while for T–Nb_2O_5, the capacity was only 76 mAh g^{-1}. Benefiting from free of carbon materials, the volumetric capacity of T–Nb_2O_5/$YbNbO_x$ at 20 C reached 132 mAh cm^{-3} considering the loading mass (2 mg cm^{-2}) and tap density (1.06 g cm^{-3}) of the material, which is among the highest values in reported Nb_2O_5 electrodes without carbon

coating,[6a,c,11] and even close to that of $Nb_{18}W_{16}O_{93}$ and $Nb_{16}W_5O_{55}$ (150 and 128 mAh g^{-1}), a kind of recently reported high energy density niobium based electrode material (Table S1).[1b] The rate retention of T–Nb_2O_5/$YbNbO_x$ under 1 C and 20 C was 80%, similar to that of $Nb_{18}W_{16}O_{93}$ (78%) and $Nb_{16}W_5O_{55}$ (80%) under same potential window of 3.0–1.2 V.[1b] Cycle stability was tested under current density of 5 C. The T–Nb_2O_5/$YbNbO_x$ electrode showed higher initial capacity of 155 mAh g^{-1}, and pure T–Nb_2O_5 electrode has a capacity of 140 mAh g^{-1}. $YbNbO_x$ coated electrode also possessed more stable cycling performance. The cycle retention of T–Nb_2O_5/$YbNbO_x$ was 88% and pure T–Nb_2O_5 was 80% within 100 cycles (Figure 4d). Considering the Coulombic efficiency of both electrodes quickly increased to 100% after initial few cycles, the enhancement of cycle stability can only be attributed to the more stable structure with $YbNbO_x$ coating (Figure S4). In order to examine the difference in diffusion behavior of lithium ions in both electrodes, we carried out GITT test to calculate the diffusion coefficients at various discharge state (Figure 4e). It can be seen from Figure 4f that both electrodes have a slope-like trend at various state of lithium insertion, indicating a solid-solution charge storage mechanism without phase transition. The diffusion coefficients of T–Nb_2O_5/$YbNbO_x$ were higher than pure Nb_2O_5 at each state of discharge. The capacitive contribution of $YbNbO_x$ coated Nb_2O_5 was 78.2%, much larger than pure Nb_2O_5 electrode (46.6%) (Figure S5). The results indicated that the lithium migration hindrance was decreased by $YbNbO_x$ coating, which finally resulted in enhanced rate performance.

As it is justified by XRD, the amorphous $YbNbO_x$ layer has significant influence on T–Nb_2O_5. There is highly possible that there is surface doping of Yb in T–Nb_2O_5 at the interface and forms the amorphous coating layer. We took X-ray absorption spectroscopy to study the local coordination structure of ytterbium. The X-ray absorption fine structure (EXAFS) and its corresponding Fourier transform are given in Figure 5a and Figure S1b, respectively. The simulated curve fitted well with experimental results, indicating the structural model in Figure 5b was reasonable, the simulated EXAFS model is shown in Figure 5b, which corresponds to monoclinic $YbNbO_4$ phase. This is an indication that the Yb element reacts with Nb_2O_5 and forms amorphous $YbNbO_x$. This hypothesis corresponded well with the XRD results that increasing Yb^{3+} doping amount would reduce the crystallinity of T–Nb_2O_5 because more amorphous oxide generates. On the one hand, the oxygen vacancy in the amorphous oxide possibly accelerated the lithium ion transport at the interface, and therefore enhanced rate performance.[12] On the other, the electric conductivity of $YbNbO_x$ is significantly higher than T–Nb_2O_5 (Figure S2). The formation of electric conductive oxide coating can be attributed as the main reason for enhanced electrochemical performance.

Besides ytterbium, we also used other rare-earth elements (neodymium, samarium, and gadolinium) as additives in T–Nb_2O_5. The rare-earth elements addition also has positive effect. By carefully tuning the doping concentration, neodymium, samarium, gadolinium and ytterbium doped samples

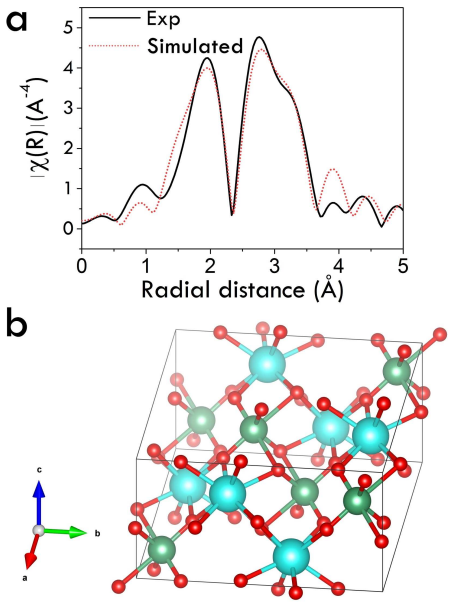

Figure 5. (a) The Yb L_3-edge EXAFS spectrum in R space. (b) the possible coordination of Yb according to EXAFS fitting. Large cyan sphere: Ytterbium; Olivine sphere: Niobium; Small red sphere: Oxygen.

achieved much better rate performance compared with pure Nb_2O_5 at each current density (Figure S3). Higher doping amount might lead to inferior performance due to high molar weight of rare-earth elements (Figure S6).

In summary, T–Nb_2O_5 with amorphous $YbNbO_x$ coating was systematically investigated. The formation of the amorphous $YbNbO_x$ layer can greatly enhance the rate performance of T–Nb_2O_5. Yb atom was possibly doped in T–Nb_2O_5 structure at Nb_2O_5/$YbNbO_x$ interface as substitutional atom. The doping of rare-earth elements did not induce structural deformation of the original lattice. Finally, we found that other rare-earth elements including Nd, Sm, and Gd also have positive effect on the rate performance. In general, it can be claimed that addition of rare-earth elements can uniquely form a thin amorphous oxide layer, which was depicted as an effective method to intrinsically enhance the rate performance of T–Nb_2O_5. Also, different from traditional doping strategy, the surface modification of electrode by rare-earth elements seems to be a promising way towards high performance energy storage materials.

Acknowledgements

We gratefully acknowledge the support from the China National Funds for Excellent Young Scientists (grant no. 21522106) and National Natural Science Foundation of China (grant no. 21971117), 111 Project (B18030) from China, and the Open Funds (RERU2019001) of the State Key Laboratory of Rare Earth Resource Utilization and the Functional Research Funds for the Central Universities, Nankai University (ZB19500202). We thank the Instrument Analysis Center of Xi'an Jiaotong University for their assistance on characterizations. Electron Microscopy (EM) work

used resources of the Center for Functional Nanomaterials, which is a US DOE Office of Science Facility, at Brookhaven National Laboratory under Contract No. DE-SC0012704.

Conflict of Interest

The authors declare no conflict of interest.

Keywords: rare-earth elements · lithium-ion battery · niobium oxide · high rate

[1] a) K. J. Griffith, A. C. Forse, J. M. Griffin, C. P. Grey, *J. Am. Chem. Soc.* **2016**, *138*, 8888–8899; b) K. J. Griffith, K. M. Wiaderek, G. Cibin, L. E. Marbella, C. P. Grey, *Nature* **2018**, *559*, 556–563; c) D. Cao, Z. Yao, J. Liu, J. Zhang, C. Li, *Energy Storage Mater.* **2018**, *11*, 152–160.

[2] D. Chen, J. H. Wang, T. F. Chou, B. Zhao, M. A. El-Sayed, M. Liu, *J. Am. Chem. Soc.* **2017**, *139*, 7071–7081.

[3] a) E. Lim, H. Kim, C. Jo, J. Chun, K. Ku, S. Kim, H. I. Lee, I. S. Nam, S. Yoon, K. Kang, J. Lee, *ACS Nano* **2014**, *8*, 8968–8978; b) X. Wang, G. Li, Z. Chen, V. Augustyn, X. Ma, G. Wang, B. Dunn, Y. Lu, *Adv. Energy Mater.* **2011**, *1*, 1089–1093; c) S. Hemmati, G. Li, X. Wang, Y. Ding, Y. Pei, A. Yu, Z. Chen, *Nano Energy* **2019**, *56*, 118–126; d) C. Shi, K. Xiang, Y. Zhu, X. Chen, W. Zhou, H. Chen, *Electrochim. Acta*, **2017**, *246*, 1088–1096.

[4] a) E. Lim, C. Jo, H. Kim, M. H. Kim, Y. Mun, J. Chun, Y. Ye, J. Hwang, K. S. Ha, K. C. Roh, K. Kang, S. Yoon, J. Lee, *ACS Nano* **2015**, *9*, 7497–7505; b) L. Kong, C. Zhang, J. Wang, W. Qiao, L. Ling, D. Long, *ACS Nano* **2015**, *9*, 11200–11208; c) J. Zhang, H. Chen, X. Sun, X. Kang, Y. Zhang, C. Xu, Y. Zhang, *J. Electrochem. Soc.* **2017**, *164*, A820-A825.

[5] H. Sun, L. Mei, J. Liang, Z. Zhao, C. Lee, H. Fei, M. Ding, J. Lau, M. Li, C. Wang, X. Xu, G. Hao, B. Papandrea, I. Shakir, B. Dunn, Y. Huang, X. Duan, *Science* **2017**, *356*, 599–604.

[6] a) J. Y. Cheong, J. W. Jung, D. Y. Youn, C. Kim, S. Yu, S.-H. Cho, K. R. Yoon, I. D. Kim, *J. Power Sources* **2017**, *360*, 434–442; b) M. M. Rahman, R. A. Rani, A. Z. Sadek, A. S. Zoolfakar, M. R. Field, T. Ramireddy, K. Kalantar-Zadeh, Y. Chen, *J. Mater. Chem. A* **2013**, *1*, 11019–11025; c) M. Liu, C. Yan, Y. Zhang, *Sci. Rep.* **2015**, *5*, 8326; d) A. L. Viet, M. V. Reddy, R. Jose, B. V. R. Chowdari, S. Ramakrishna, *J. Phys. Chem. C* **2010**, *114*, 664–671; e) H. Chen, H. Zhang, Y. Wu, T. Zhang, Y. Guo, Q. Zhang, Y. Zeng, J. Lu, *J. Electroanal. Chem.*, **2018**, *827*,112-119.

[7] a) V. Augustyn, J. Come, M. A. Lowe, J. W. Kim, P. L. Taberna, S. H. Tolbert, H. D. Abruña, P. Simon, B. Dunn, *Nat. Mater.* **2013**, *12*, 518–522; b) J. Wang, J. Polleux, J. Lim, B. Dunn, *J. Phys. Chem. C* **2007**, *111*, 14925–14931.

[8] a) J. Mei, T. F. Yi, X. Y. Li, Y. R. Zhu, Y. Xie, C. F. Zhang, *ACS Appl. Mater. Interfaces* **2017**, *9*, 23662–23671; b) Y. Gao, R. L. Patel, K. Y. Shen, X. Wang, R. L. Axelbaum, X. Liang, *ACS Omega* **2018**, *3*, 906–916; c) R. L. Patel, H. Xie, J. Park, H. Y. Asl, A. Choudhury, X. Liang, *Adv. Mater. Interfaces* **2015**, *2*, 1500046; d) Y. Q. Wang, L. Gu, Y. G. Guo, H. Li, X. Q. He, S. Tsukimoto, Y. Ikuhara, L. J. Wan, *J. Am. Chem. Soc.* **2012**, *134*, 7874–7879.

[9] J. C. Bachman, S. Muy, A. Grimaud, H.-H. Chang, N. Pour, S. F. Lux, O. Paschos, F. Maglia, S. Lupart, P. Lamp, L. Giordano, Y. Shao-Horn, *Chem. Rev.* **2016**, *116*, 140–162.

[10] a) L. Ye, S. Xie, B. Yue, L. Qian, S. Feng, S. C. Tsang, Y. Li, H. He, *CrystEngComm* **2010**, *12*, 344–347; b) P. Yang, D. Zhao, D. I. Margolese, B. F. Chmelka, G. D. Stucky, *Chem. Mater.* **1999**, *11*, 2813–2826.

[11] a) S. Li, C. N. Schmidt, Q. Xu, X. Cao, G. Cao, *ChemNanoMat* **2016**, *2*, 675–680; b) H. Yang, H. Xu, L. Wang, L. Zhang, Y. Huang, X. Hu, *Chem. Eur. J.* **2017**, *23*, 4203–4209; c) G. Luo, H. Li, D. Zhang, L. Gao, T. Lin, *Electrochim. Acta* **2017**, *235*, 175–181.

[12] a) T. Koketsu, J. Ma, B. J. Morgan, M. Body, C. Legein, W. Dachraoui, M. Giannini, A. Demortière, M. Salanne, F. Dardoize, H. Groult, O. J. Borkiewicz, K. W. Chapman, P. Strasser, D. Dambournet, *Nat. Mater.* **2017**, *16*, 1142–1148; b) H. S. Kim, J. B. Cook, H. Lin, J. S. Ko, S. H. Tolbert, V. Ozolins, B. Dunn, *Nat. Mater.* **2016**, *16*, 454–460.

Manuscript received: May 11, 2019
Revised manuscript received: July 14, 2019
Accepted manuscript online: August 16, 2019
Version of record online: September 2, 2019